Weierstraß-Institut
für Angewandte Analysis und Stochastik

im Forschungsverbund Berlin e.V.

Linear stability analysis of a sharp-interface model for dewetting thin films

John R. King[1], Andreas Münch[2] and Barbara Wagner[3]

submitted: July 20, 2007

[1]   University of Nottingham,
      Theoretical Mechanics Section, School of Mathematical Scienses
      Nottingham NG7 2RD, UK

[2]   Humboldt University of Berlin,
      Institute of Mathematics, D-10099 Berlin

[3]   Weierstrass Institute for Applied Analysis and Stochastics (WIAS),
      Mohrenstraße 39, D-10117 Berlin

Abstract

The topic of this study concerns the stability of the three-phase contact-line of a dewetting thin liquid film on a hydrophobised substrate driven by van der Waals forces. The role of slippage in the emerging instability at the three-phase contact-line is studied by deriving a sharp-interface model for the dewetting thin film via matched asymptotic expansions. This allows for a derivation of travelling waves and their linear stability via eigenmode analysis. In contrast to the dispersion relations typically encountered for the finger-instabilty, where the dependence of the growth rate on the wave number is quadratic, here it is linear. Using the separation of time scales of the slowly growing rim of the dewetting film and time scale on which the contact line destabilises, the sharp-interface results are compared to earlier results for the full lubrication model and good agreement for the most unstable modes is obtained.

1   Introduction

Contact-line instabilities for thin liquid films that wet a solid substrate have been studied for decades, both theoretically and experimentally. The instabilities are typically driven by forces such as gravity [1, 19, 44, 46], Marangoni stresses or both [2, 6, 8, 14, 21]. The derivation of reduced mathematical models exploits a separation of length scales to obtain a simplified lubrication model from the underlying Navier-Stokes equations in conjunction with conservation of mass. The stress singularity at the three phase contact line, which is inherited by the resulting fourth-order partial differential equation, is regularized for example via a slip boundary condition or precursor model, where the height of the precursor or the slip length is usually much smaller than the height of the actual wetting film. The choice of the boundary condition at the three phase contact line typically enters only weakly in that it does not influence the eventual appearance of fingers: see for example [1, 21, 24, 29].

In contrast to the wetting scenarios the film thickness in dewetting experiments is typically smaller by orders of magnitude. The physical situation consists of a thin viscous polymer film that is uniformly spread on a substrate such as a silicon wafer with a hydrophobic coating. For such a multi-layered system one can reconstruct the disjoining pressure from a corresponding inter-molecular potential which is composed of repulsive and attractive long-range van der Waals contributions and a short-range term which accounts for Born-type repulsion, see e.g. [39, 40]. The latter term provides a cut-off by penalizing a thinning of the film below a positive thickness threshold given by the minimum of the potential. For such a situation the thin film dewets in a process that is initiated either spontaneously through spinodal decomposition or

induced through nucleation for example. The dry spots, or holes, that form as a result subsequently grow as the newly formed contact line recedes, thereby accumulating liquid in a characteristic capillary ridge at the edge of the hole, which increases in width and height as the dewetting proceeds. In a variety of experimental situations it is observed that, while in some cases the growth of the hole continues until it collides with neighboring holes, in others the ridge of the hole destabilizes into finger-like structures eventually pinching off and forming droplets. Such finger-like contact-line instabilities have also been observed for straight dewetting fronts as opposed to radially symmetric fronts, see [23, 31, 35, 38, 41, 42, 48]. Because of the impact this has on the emerging macroscopic pattern, it is important to understand the dynamics leading to such an instability.

For such situations, the relevance of slippage at the liquid/solid interface for the instability have been discussed by several authors, [25, 28, 30, 37, 43]. In [3, 20, 33] the dewetting rate and shape of the ridge has been treated using approximate formulas derived from scaling arguments and energy balances. However, in order to capture the dynamics of the contact-line instability it is convenient to describe the evolution of the film surface $z = h(x, y, t)$ via a lubrication approximation that includes the influence of surface tension and the intermolecular potential $\phi(h)$ of the air/liquid/solid layer. Coordinates are introduced here so that x, y denote the directions parallel to the substrate, and z the direction normal to it. In this case the pressure at $z = h(x, y, t)$ is given by

$$p = -\Delta h + \phi'(h). \tag{1.1}$$

where $\phi'(h)$ is the first derivative of the intermolecular potential with respect to the liquid film thickness h. A typical choice for $\phi(h)$, and the one we will adopt in this paper, is [39]

$$\phi'(h) = \epsilon^{-1}\Phi'(h/\epsilon), \quad \text{where} \quad \Phi(h) = \frac{1}{8h^8} - \frac{1}{2h^2}. \tag{1.2}$$

Note that $\Phi'(1) = 0$ and $\Phi''(1) > 0$, so that ϕ has a minimum at $h = \epsilon \ll 1$. This implies that very thin films with a thickness scale of ϵ are energetically preferred to in particular thicker films which therefore tend to dewet. Making use of the length scale separation in the x, y vs. z direction, one can then derive the lubrication model [32] from the Navier-Stokes equation and (1.1)

$$h_t + \nabla \cdot \left[h^n \nabla \left(\Delta h - \phi'(h) \right) \right] = 0, \tag{1.3}$$

stated here (as are all equations in this paper) in non-dimensional form. Here h^n is the mobility coefficient, where the power n depends on the boundary conditions at the liquid/solid interface. A widely used condition relates the slippage velocity u of the liquid at the wall to the local shear rate u_z via

$$u = b\, u_z, \tag{1.4}$$

where the slip length b can be thought of as the distance below the interface at which the liquid velocity extrapolates to zero. For the above slip boundary
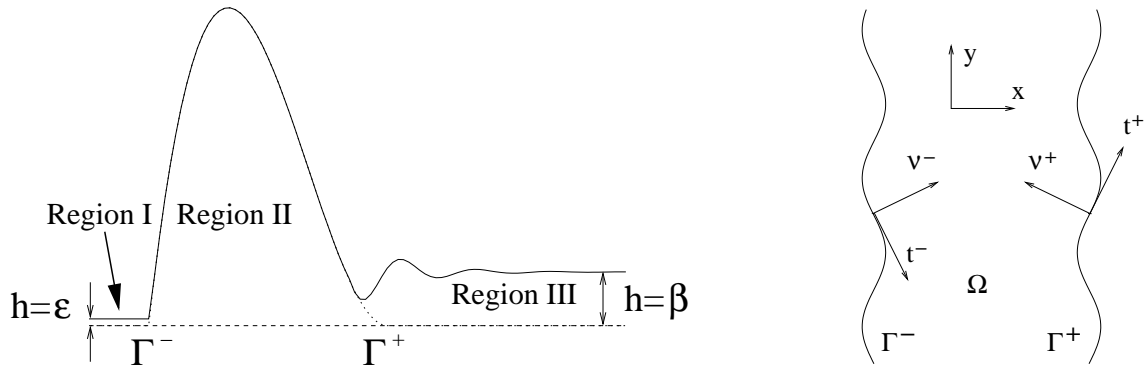
2

Figure 1: (a) Sketch of a cross section of a dewetting rim. (b) Sketch of a top view of a (perturbed) ridge for a sharp-interface model, showing the domain Ω occupied by the ridge and the two free boundary curves $\Gamma^{\pm}$.

condition at the substrate, the typically used no-slip boundary condition is obtained if $b = 0$. On the other hand, stuying the hydrodynamic eaquations for different orders of magnitude of b it was shown, using asymptotic analysis [30], that a hierarchy of lubrication models emerge. One of them with the mobility h^2 has the distinct property that it describes dewetting films with a dewetting rate of $t^{1/3}$, [27]. For this case travelling-wave solutions were derived using matched asymptotic expansions [30]. In [28] a linear stability analysis showed that small perturbations of the receding front are amplified, but in the slip case by orders of magnitude larger than in the no-slip case. Moreover, while the perturbations become symmetrical in the no-slip case, they are asymmetrical and in [26] it was shown that these properties carry over into the nonlinear regime of the lubrication models. In the context of lubrication models for dewetting thin films [13] derived asymptotic solutions for the shape of the dewetting ridges, their dewetting rates and for the limiting case of the mobility h^3 their contact-line instability was investigated via matched asymptotic expansions. In this study we will investigate the linear stability of the contact-line for the lubrication model with mobility h^2 by deriving first a sharp-interface model. This also enables us to separate the slow growth of the rim from the faster time-scale on which the contact line destabilizes. As a result, the linear stability analysis can be reduced to an eigenvalue analysis. Note here that in the context of spreading liquid droplets, [15, 16, 17] introduced a variational approach leading to reduced models for the motion of the contact line for the no-slip case.

We begin our study by first deriving the sharp-interface model in section 2. The we first derive their travelling waves in section 3 and study their stability in section 4. Finally we compare our results the those for the full lubrication model studied in [26, 28].

3

2 Derivation of the sharp-interface model

2.1 Outer Problem

We consider here equation (1.3) for $n = 2$, i.e.

$$h_t + \nabla \cdot \left[h^2 \nabla \cdot \left(\triangle h - \varepsilon_1^{-1} \Phi' \left(h/\varepsilon_1 \right) \right) \right] = 0, \tag{2.1}$$

and far field conditions

$$\lim_{x \to -\infty} h(x, y, t) = \varepsilon_1, \quad \text{and} \quad \lim_{x \to +\infty} h(x, y, t) = 1, \tag{2.2}$$

where $\varepsilon_1 \ll 1$. This formulation is convenient, for example, for numerical simulations, where the unperturbed film thickness is held fixed and the growth of the rim is observed. For the derivation of the sharp interface model, it is important that both the residual film on the left and the unperturbed film on the right are much smaller in height of than the actual rim. Therefore, we rescale the film profile h by a quantity $1/\beta$ that is large compared to the unperturbed film thickness, i.e., $\beta << 1$, but at most of the order of the typical ridge height. To maintain the form of the governing equation and the potential, the other variables are scaled accordingly, i.e.

$$h = \frac{1}{\beta} \tilde{h}, \quad x = \frac{1}{\beta} \tilde{x}, \quad y = \frac{1}{\beta} \tilde{y}, \quad t = \frac{1}{\beta^2} \tilde{t}. \tag{2.3}$$

Introducing these scalings yields, after dropping $\sim$'s,

$$h_t + \nabla \cdot \left[h^2 \nabla \cdot \left(\triangle h - \varepsilon^{-1} \Phi' \left(h/\varepsilon \right) \right) \right] = 0, \tag{2.4}$$

and far field conditions

$$\lim_{x \to -\infty} h(x, y, t) = \varepsilon, \quad \text{and} \quad \lim_{x \to +\infty} h(x, y, t) = \beta, \tag{2.5}$$

where $\varepsilon \equiv \varepsilon_1 \beta \ll \beta \ll 1$. This is the appropriate outer scaling for the subsequent derivations.

2.2 Transformation to inner coordinates near the contact line

Let $\mathbf{x} = (x, y)$ be a point in the neighborhood of the contact line Γ^-, parametrized by $\mathbf{r}^-(t, s) = (r_1^-(t, s), r_2^-(t, s))$, where s denotes arclength. Then

$$\mathbf{x} = \mathbf{r}^-(t, s) + \varepsilon \chi \boldsymbol{\nu}(t, s) \tag{2.6}$$

defines the boundary layer with χ being the boundary layer or 'inner' variable. The normal $\boldsymbol{\nu}(t, s) = (-r_{2s}^-(t, s), r_{1s}^-(t, s))$ and the tangential unit vector $\mathbf{t}(t, s) = (r_{1s}^-(t, s), r_{2s}^-(t, s))$ are chosen so that $(\mathbf{t}, \boldsymbol{\nu})$ is a right hand system, and $\boldsymbol{\nu}$ points into the ridge, i.e. into Ω, see figure 1(b). In the inner region the height is much smaller and we set

$$h = \varepsilon v \tag{2.7}$$

4

Making use of appendix A in [22] we obtain the expression

$$
\begin{aligned}
\nabla \cdot \left(h^2 \nabla p \right) \;=\; & \varepsilon^2 \left[2v \left(r_{1s}^-(1 - \varepsilon \chi \kappa) v_s + \varepsilon^{-1} r_{2s}^- v_\chi \right) \left(r_{1s}^-(1 - \varepsilon \chi \kappa) p_s + \varepsilon^{-1} r_{2s}^- p_\chi \right) \right. \\
& +2v \left(r_{2s}^-(1 - \varepsilon \chi \kappa) v_s - \varepsilon^{-1} r_{1s}^- v_\chi \right) \left(r_{2s}^-(1 - \varepsilon \chi \kappa) p_s - \varepsilon^{-1} r_{1s}^- p_\chi \right) \\
& \left. +v^2 \left(\varepsilon^{-2} p_{\chi\chi} + \varepsilon^{-1} \kappa p_\chi + p_{ss} - \chi \kappa^2 p_\chi \right) \right]
\end{aligned}
\tag{2.8}
$$

where

$$
p = -\varepsilon^{-1} \left(v_{\chi\chi} - \Phi'(v) \right) - \kappa v_\chi - \varepsilon \left(v_{ss} - \chi \kappa^2 v_\chi \right)
\tag{2.9}
$$

Hence, to leading order in ε the second term of (2.4) is

$$
\nabla \cdot \left(h^2 \nabla p \right) \sim \varepsilon^{-1} \left[v^2 \left(v_\chi - \Phi'(v) \right) \right]_\chi
\tag{2.10}
$$

Since the first term of (2.4) is transformed to

$$
h_t = -\varepsilon V^{\mathbf{t}} (1 - \varepsilon z \kappa) v_s + V^{\boldsymbol{\nu}} v_z + \varepsilon v_t
\tag{2.11}
$$

the leading order the inner problem becomes

$$
\left[v^2 \left(v_{\chi\chi} - \Phi'(v) \right) \right]_\chi = 0
\tag{2.12}
$$

together with the boundary conditions

$$
\lim_{\chi \to -\infty} v = 1, \quad \lim_{\chi \to -\infty} v_\chi = 0, \quad \lim_{\chi \to -\infty} v_{\chi\chi} = 0 \,.
\tag{2.13}
$$

Integrating (2.13) twice, using the fact that the potential satisfies $\Phi'(1) = 0$ since Φ has a minimum there, we get $v_{\chi\chi} = \Phi'(v)$, hence

$$
v_\chi = 2^{1/2} \left(\Phi(v) - \Phi(1) \right)^{1/2} .
\tag{2.14}
$$

For matching we need the behavior for large χ, which is

$$
v_\chi \to 2^{1/2} \left(-\Phi(1) \right)^{1/2} \equiv \lambda \quad \text{as} \quad \chi \to \infty.
\tag{2.15}
$$

Transformation back to outer variables via

$$
v = \chi \lambda \,, \quad \text{where} \quad \chi = \frac{(\mathbf{x} - \mathbf{r}) \cdot \boldsymbol{\nu}}{\varepsilon},
$$

yields

$$
h = (\mathbf{x} - \mathbf{r}) \cdot \boldsymbol{\nu} \, \lambda.
\tag{2.16}
$$

The sharp-interface model then results from the leading order outer problem, together with the boundary condition found by matching to (2.16),

$$
h_t \;=\; -\nabla \cdot \left(h^2 \nabla \triangle h \right), \quad \text{in} \quad \Omega
\tag{2.17}
$$

$$
\frac{\partial h}{\partial \boldsymbol{\nu}} \;=\; \lambda, \quad h = 0, \quad h \frac{\partial}{\partial \boldsymbol{\nu}} \triangle h - V_\nu^- = 0 \quad \text{on } \Gamma^-,
\tag{2.18}
$$

where the third boundary condition in (2.18) arises by letting $\chi \to \infty$, $v \to \infty$ in (2.12). In (2.18), we have introduced the notation

$$
V_\nu^- \equiv \mathbf{r}_t^- \cdot \boldsymbol{\nu}.
\tag{2.19}
$$

Next, we derive the boundary condition on Γ^+.

2.3 Transformation to inner coordinates near undisturbed film

Here we let $\mathbf{x} = (x, y)$ be a point in the neighborhood of the sharp interface Γ^+, parametrized by $\mathbf{r}^+(t, s) = (r_1^+(t, s), r_2^+(t, s))$. Then

$$\mathbf{x} = \mathbf{r}^+(t, s) + \beta^\gamma \zeta \boldsymbol{\nu}(t, s) \tag{2.20}$$

defines the boundary layer with ζ being the 'inner' variable, where the scaling exponent γ remains to be determined. As before, the normal unit vector $\boldsymbol{\nu}(t, s) = (-r_{2s}^+(t, s), r_{1s}^+(t, s))$ points into ridge (figure 1(b)) and the tangential unit vector $\mathbf{t}(t, s) = (r_{1s}^+(t, s), r_{2s}^+(t, s))$ is chosen so that $(\mathbf{t}, \boldsymbol{\nu})$ form a right hand system.

In this second inner region we set

$$h = \beta u \tag{2.21}$$

To leading order in β we find for h_t the expression

$$h_t \sim -\beta^{1-\gamma} V^{\boldsymbol{\nu}} u_\zeta \sim -\beta^{1-\gamma} \left(\mathbf{r}_t^+ \cdot \boldsymbol{\nu}\right) u_\zeta \tag{2.22}$$

and we have

$$\nabla \cdot \left(h^2 \nabla \left(\triangle - \varepsilon^{-1} \Phi\left(h/\varepsilon\right)\right)\right) \sim \beta^{3-4\gamma} \left(u^2 \left(u_{\zeta\zeta} - \beta^{2\gamma-1} \varepsilon^{-1} \Phi\left(\beta u/\varepsilon\right)\right)_\zeta\right)_\zeta \tag{2.23}$$

A travelling-wave balance for the moving rim thus requires

$$\gamma = \frac{2}{3} \tag{2.24}$$

In order for the intermolecular forces to play no role in this region we require

$$O\left(\beta^{2\gamma-1} \varepsilon^{-1} \Phi\left(\beta u/\varepsilon\right)\right) \ll 1 \tag{2.25}$$

which introduces a restriction on β in terms of ε, namely $\varepsilon^2 \ll \beta^{8/3}$. Hence, we obtain for the leading order inner problem near the undisturbed film

$$-V_\nu^+(s, t) u_\zeta + \left(u^2 u_{\zeta\zeta\zeta}\right)_\zeta = 0 \tag{2.26}$$

where

$$V_\nu^+(s, t) \equiv \mathbf{r}_t^+ \cdot \boldsymbol{\nu} \tag{2.27}$$

This we integrate with respect to ζ and use the far field condition

$$\lim_{\zeta \to -\infty} u = 1 \tag{2.28}$$

to obtain

$$-V_\nu^+(s, t)(u - 1) + u^2 u_{\zeta\zeta\zeta} = 0 \tag{2.29}$$

For the matching to the outer problem we rescale first $\zeta = \eta/(-V_\nu^+)^{1/3}$ to obtain the equation

$$u_{\eta\eta\eta} = \frac{u - 1}{u^2}. \tag{2.30}$$

6

See for example [47], where this equation has been discussed. Note that we can assume that as long as the basic motion of the rim in outer coordinates is to the right (i.e. in the positive direction of the x-axis), $V_\nu^+(s,t)$ is *negative*, hence the orientation is not reversed by the rescaling from ζ into η variables. Therefore, the flat film far field condition and the matching conditions are imposed at $\eta \to -\infty$ and $\eta \to +\infty$, as before. Equation (2.30) has a solution with leading order behavior

$$u(\eta) \sim 2\,(2/3)^{1/2}\,\eta^{3/2} \qquad \text{as} \quad \eta \to +\infty \tag{2.31}$$

and hence

$$u(\zeta) \sim 2\,(2/3)^{1/2}\,(-V_\nu^+)^{1/2}\zeta^{3/2} \tag{2.32}$$

as $\zeta \to \infty$. In outer scales we obtain

$$h = 2\,(2/3)^{1/2}\,(-V_\nu^+)^{1/2}\Big(\left(\mathbf{x} - \mathbf{r}^+ \right) \cdot \boldsymbol{\nu} \Big)^{3/2} \tag{2.33}$$

as the appropriate matching condition.

Finally we get for the sharp-interface model

$$h_t = -\nabla \cdot \left(h^2 \nabla \triangle h \right), \quad \text{in} \quad \Omega \tag{2.34a}$$

$$h = 0\,, \quad \frac{\partial h}{\partial \boldsymbol{\nu}} = \lambda\,, \quad h\frac{\partial}{\partial \boldsymbol{\nu}}\triangle h - V_\nu^- = 0 \quad \text{on } \Gamma^-, \tag{2.34b}$$

$$h \sim 2\,(2/3)^{1/2}\,(-V_\nu^+)^{1/2}\Big(\left(\mathbf{r}^+ - \mathbf{x} \right) \cdot \boldsymbol{\nu} \Big)^{3/2} \quad \text{as } x \to \mathbf{r}^+ \tag{2.34c}$$

For the subsequent discussion of the sharp-interface model it is convenient to introduce the parametrization of Γ^- and Γ^+ as graphs of functions of $s^-(y,t)$ and $s^+(y,t)$, i.e. $y \mapsto (-y, -s^-(y,t))$ and $y \mapsto (y, s^+(y,t))$, respectively. We obtain the following expressions for the tangent and normal unit vectors

$$\mathbf{t}^- = \frac{(-s_y^-, -1)}{\sqrt{\left(s_y^-\right)^2 + 1}} \quad \text{and} \quad \boldsymbol{\nu}^- = \frac{(1, -s_y^-)}{\sqrt{\left(s_y^-\right)^2 + 1}}\,, \tag{2.35}$$

on Γ^-, and

$$\mathbf{t}^+ = \frac{(s_y^+, 1)}{\sqrt{\left(s_y^+\right)^2 + 1}} \quad \text{and} \quad \boldsymbol{\nu}^+ = \frac{(-1, s_y^+)}{\sqrt{\left(s_y^+\right)^2 + 1}}\,, \tag{2.36}$$

on Γ^+.

3 Travelling-wave solutions

We now assume that the base state is a travelling wave that moves with constant speed c and does not depend on y. The ansatz is $h = h_0(\bar{x})$, where $\bar{x} = x - ct$, and $\bar{s}_0^\pm = s_0^\pm - ct$, with constant $\bar{s}_0^\pm$ (i.e. independent of $\bar{x}$, y or t). Inserting the new variables, we obtain, after dropping the bars,

$$h_0 h_{0xxx} = c\,, \tag{3.1a}$$

$$h_0 = 0\,, \quad h_{0x} = \lambda\,, \quad h_0^2 h_{0xxx} = 0 \quad \text{on } x = s_0^-\,, \tag{3.1b}$$

$$h_0 \sim 2\,(2/3)^{1/2}\,c^{1/2}\left(s_0^+ - x\right)^{3/2} \quad \text{for } x \to s_0^+\,. \tag{3.1c}$$

7

Here we have integrated the resulting ODE once and used the boundary conditions to fix the constant of integration.

We can rescale (3.1a)-(3.1c) to eliminate c and λ via

$$h_0 = (\lambda^3/c)\varphi_0, \quad x = (\lambda^2/c)\xi + s_0^-, \quad s_0^+ = (\lambda^2/c)d + s_0^-, \qquad (3.2)$$

which yields (with $' = d/d\xi$):

$$\varphi_0\varphi_0''' = 1, \qquad\qquad\qquad (3.3a)$$
$$\varphi_0 = 0, \quad \varphi_0' = 1, \quad \varphi_0^2\varphi_0''' = 0 \quad \text{on } \xi = 0, \qquad (3.3b)$$
$$\varphi_0 \sim 2\,(2/3)^{1/2}\,(d-\xi)^{3/2} \quad \text{for} \quad \xi \to d. \qquad (3.3c)$$

Note that this can be integrated to

$$\varphi_0\varphi_0'' - \frac{1}{2}\varphi_0^2 = \xi - d. \qquad (3.4)$$

We now discuss solutions of (3.3). Note first that the function on the right hand side of (3.3c) is itself an exact solution of the ODE (3.3a). The general expansion for solutions of (3.3a) with the leading-order behaviour at $\xi = d$ required by (3.3c) suggests a one-parameter (in addition to d) family of solutions and is given by

$$\varphi_0(\xi) = 2\,(2/3)^{1/2}\,(d-\xi)^{3/2} + a^+(d-\xi)^{3/2+\mu} + \sum_{n=2}^{\infty} a_n^+(d-\xi)^{3/2+\mu n} \quad (3.5)$$

Here, μ denotes the constant $\mu = \left(-1 + \sqrt{13}\right)/4$ and a^+ is a free parameter. The coefficients a_n^+ must be determined recursively from the ODE for $n \geq 2$.

Similarly, at $\xi = 0$, we have a one parameter family of solutions that satisfy the relevant boundary conditions (3.3b). In fact, in [7], Buckingham et al. find a general series expansion for (3.3a) at $\xi = 0$ that satisfies $h(0) = 0$ with two free parameters. Using the form given by the authors and enforcing the boundary conditions (3.3b) to fix one of the two free parameters, we obtain

$$\varphi_0(\xi) = \xi + (1/2)\xi^2\ln\xi + a^-\xi^2 + \sum_{n=3}^{\infty}\sum_{m=2}^{n} a_{nm}^-\xi^n(\ln\xi)^{n-m} \quad \text{at } \xi = 0. \quad (3.6)$$

Here, a^- is the remaining free parameter, and the a_{mn}^- must be determined recursively from the ODE.

In summary, we have, for each boundary point a two-dimensional invariant manifold of trajectories in the three-dimensional phase space of (3.3a). Solutions of (3.3) arise from intersections of these manifolds. These are co-dimension one Intersections so that we expect a discrete family of solutions, for a discrete family of d. In fact, as pointed out by [13], upon integrating (3.3a) once and imposing the boundary conditions, one fixes the constant of integration and also obtain a single value for d,
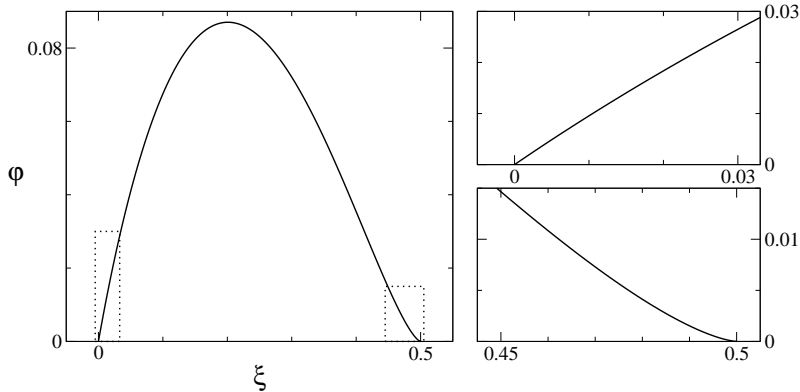
$$d = \frac{1}{2}. \qquad (3.7)$$

Figure 2: The normalized base state for the base state of the slip model, obtained as numerical solution of (3.3).

We solved this problem numerically, using LSODE [18] to solve (3.3a) with initial conditions obtained from the series expansion imposed at $\xi = \xi_1$ and $\xi = 1/2 - \xi_1$, with a small ξ_1. Continuity of the solution and its derivative was imposed at the mid point $\xi = 1/4$ and these conditions solved numerically for a^- and a^+ by Newton iterations. We obtained $a^- = -2.175$ and $a^+ = -2.226$. The solution φ_0 is shown in figure 2.

4   Linear stability

4.1   Formulation

We first shift the governing equations of the sharp-interface model (2.34) to the moving frame of reference also used in (3.1), by letting $\bar{x} = x - ct$, and $\bar{s}^\pm = s^\pm - ct$, where now $\bar{s}^\pm$ may be a non-constant function depending on y and t. After introducing the new variables, we drop the bars to give

$$h_t - ch_x + \nabla \cdot (h^2 \nabla \triangle h) = 0 \,, \tag{4.1a}$$

$$h = 0 \,, \quad \frac{h_x - h_y s_y^-}{\left(1 + (s_y^-)^2\right)^{1/2}} = \lambda,$$

$$h^2 \frac{\triangle h_x - \triangle h_y s_y^-}{\left(1 + (s_y^-)^2\right)^{1/2}} - \frac{(s_t^- + c)\, h}{\left(1 + (s_y^-)^2\right)^{1/2}} = 0, \quad \text{for } x = s_y^-, \tag{4.1b}$$

$$h \sim 2\,(2/3)^{1/2} \left(\frac{s_t^+ + c}{\left(1 + (s_y^+)^2\right)^{1/2}}\right)^{1/2} \left(\frac{s^+ - x}{\left(1 + (s_y^+)^2\right)^{1/2}}\right)^{3/2} \quad \text{as} \quad x \to s^+. \tag{4.1c}$$

To address linear stability we now let

$$s^\pm \sim \pm s_0 + \beta s_1^\pm(t)\, e^{iky}, \quad h \sim h_0 + \beta h_1(x,t)\, e^{iky}, \tag{4.2}$$

where h_0, $s_0^\pm$ denotes the solution of (3.1) obtained in the previous section 3, which serves as our base state. To $O(\beta)$ we get

$$h_{1t} - ch_{1x} + \left[h_0^2(h_{1xxx} - k^2 h_{1x})\right]_x - k^2 h_0^2(h_{1xx} - k^2 h_1) = 0 \tag{4.3}$$

9

with boundary conditions

$$h_1 + \lambda \, s_1^- \;=\; 0\,, \tag{4.4a}$$

$$h_{1x} + h_{0xx} \, s_1^- \;=\; 0\,, \tag{4.4b}$$

$$h_0^2 h_{1xxx} - c h_1 \;=\; 0\,, \tag{4.4c}$$

as $x \to s_0^-$ and

$$h_1 \sim 6^{1/2} c^{1/2} s_1^+ \left(s_0^+ - x\right)^{1/2} \tag{4.5}$$

as $x \to s_0^+$.

We make the ansatz

$$[\, s_1^\pm(t), h_1(x,t)\,] = [\, \hat{s}^\pm, \, \hat{h}(x)\,] \, e^{\alpha t} \tag{4.6}$$

and obtain from (4.3)-(4.5) and the variable transformation

$$x = \frac{\lambda^2}{c}\xi + s_0^-\,, \quad k = \frac{c}{\lambda^2}\, q, \tag{4.7a}$$

$$s_0^+ = \frac{\lambda^2}{2c} + s_0^-\,, \quad s_1^- = \frac{\lambda^2}{c}d_1^-\,, \quad s_1^+ = \frac{\lambda^2}{c}d_1^+\,, \tag{4.7b}$$

$$h_0 = \frac{\lambda^3}{c}\varphi_0, \quad h_1 = \frac{\lambda^3}{c}\varphi_1, \quad \alpha = \frac{c^2}{\lambda^2}\, \sigma, \tag{4.7c}$$

the eigenvalue problem

$$-\sigma\varphi_1 \;=\; \left(\varphi_0^2 \left(\varphi_{1\xi\xi} - q^2\varphi_1\right)_\xi\right)_\xi - q^2\varphi_0^2 \left(\varphi_{1\xi\xi} - q^2\varphi_1\right) + \varphi_{1\xi}, \tag{4.8a}$$

$$\varphi_{1\xi} \;=\; \varphi_{0\xi\xi}\varphi_1\,, \quad \varphi_0^2\varphi_{1\xi\xi\xi} - \varphi_1 = 0, \quad \text{at} \quad \xi = 0, \tag{4.8b}$$

$$\varphi_1 \;\sim\; 6^{1/2}d_1^+ \left(1/2 - \xi\right)^{1/2} \quad \text{as} \quad \xi \to 1/2, \tag{4.8c}$$

where φ_0 is the rescaled base state, i.e. the solution of (3.3). Note that we have used (4.4a), (4.4b) to eliminate s_1^- i.e. d_1^- from (4.8b). Note also that the leading behavior of $\varphi_{0\xi\xi}$ in (4.8b) can be obtained by taking derivatives of (3.6),

$$\varphi_{0\xi\xi} = \frac{3}{2} + 2a^- + \ln\xi + O(\xi\ln\xi) \quad \text{for } \xi \to 0. \tag{4.9}$$

The general solution of the linear ODE (4.8a) can be found as a linear combination of four basis functions with the following distinct types of leading-order behaviour,

$$\psi_1^- \sim 1 + o(\xi^2), \quad \psi_2^- \sim \xi + o(\xi^2), \quad \psi_3^- \sim \xi\ln\xi + o(\xi^2), \quad \psi_4^- \sim \xi^2, \quad \text{as } \xi \to 0. \tag{4.10}$$

In view also of (4.9), a linear combination $h_1 = \sum_{i=1}^4 c_i\psi_i^-$ satisfies only (4.8b) if $c_3 = c_1$ and $c_2 = (1/2 + 2a^-)\,c_1$, i.e. in effect two conditions are imposed at the boundary $\xi = 0$. The general solution of the ODE that satisfies the boundary condition is then given by

$$\varphi_1 = c_1^- \phi_1^- + c_2^- \phi_2^-\,, \tag{4.11a}$$

10

where

$$\phi_1^- = 1 + \left(\frac{1}{2} + 2a^-\right)\xi + \xi \ln \xi + O(\xi^2 \ln \xi), \tag{4.11b}$$

$$\phi_2^- = \xi^2 + O(\xi^2 \ln \xi), \tag{4.11c}$$

as $\xi \to 0$.

Similarly, the four possible leading order behaviors as $\xi \to 1/2$ are given by $(1/2 - \xi)^\rho$ with $\rho = 0$, $3/2 - \mu$, $1/2$, and $1 + \mu$, where $\mu = (1 + \sqrt{13})/4$ denotes the same constant as in section 3. Only the last two power-law behaviours are consistent with the boundary condition (4.8c), where the second last corresponds to a shift in location of the interface, i.e. we also effectively impose two conditions at the right boundary, yielding the total of four conditions required for a fourth order eigenvalue problem. The general solution of (4.8a) that satisfies (4.8c) is given by

$$\varphi_1 = c_1^+ \phi_1^+ + c_2^+ \phi_2^+, \tag{4.12a}$$

where

$$\phi_1^+ \sim (1/2 - \xi)^{1/2}, \tag{4.12b}$$

$$\phi_2^+ \sim (1/2 - \xi)^{(5 + \sqrt{13})/4}. \tag{4.12c}$$

as $\xi \to 1/2$.

4.2 Numerical construction

To obtain the eigensolutions we use use a construction based on the idea of Evans functions, [9, 10, 11, 12]. For σ to be an eigenvalue, there must exist $c_1^\pm$ and $c_2^\pm$ so that $c_1^- \phi_1^- + c_2^- \phi_2^-$ and $c_1^+ \phi_1^+ + c_2^+ \phi_2^+$ are non-zero and equal for $0 \leq \xi \leq 1/2$. Then, the common function they represent is an eigenfunction corresponding to the eigenvalue σ. The two linear combinations are equal throughout the whole interval if their value and the first three derivatives are equal at an arbitrary point of the interval. Therefore, an eigenvalue is found if the Wronskian

$$W = \det A, \qquad A = \begin{pmatrix} \phi_1^- & \phi_2^- & \phi_1^+ & \phi_2^+ \\ \left(\phi_1^-\right)' & \left(\phi_2^-\right)' & \left(\phi_1^+\right)' & \left(\phi_2^+\right)' \\ \left(\phi_1^-\right)'' & \left(\phi_2^-\right)'' & \left(\phi_1^+\right)'' & \left(\phi_2^+\right)'' \\ \left(\phi_1^-\right)''' & \left(\phi_2^-\right)''' & \left(\phi_1^+\right)''' & \left(\phi_2^+\right)''' \end{pmatrix}, \tag{4.13}$$

is zero at any point of the intervall and hence everywhere. If this is the case, the kernel of A specifies the coefficients $c_1^\pm$ and $c_2^\pm$ that determine the eigenfunction via

$$A\left(c_1^-, c_2^-, -c_2^+, -c_2^+\right)^T = 0. \tag{4.14}$$

where the superscript indicates transposition.

We used this approach to obtain the eigenvalues and eigenfunctions numerically. For given q and a given candidate eigenvalue σ, we first computed

11

the functions $\phi_1^{\pm}$, $\phi_2^{\pm}$ using LSODE. The initial conditions for the numerical solver were imposed at ξ_2 and $1/2 - \xi_2$ for a small positive ξ_2 larger than the value ξ_1 for the base state: this was done to avoid the singular or near singular behavior at the boundary points and to obtain solutions with the prescribed leading behavior there. The initial conditions were obtained from the first few terms of the series expansions of each of the four solutions, which were determined prior to the numerical computations with the aid of MAPLE. At $\xi = 1/4$, we computed the Wronskian. We restricted our attention to real eigenvalues so that the value of σ for which W vanishes could be determined by bisectioning.

We found two eigenvalues, shown in figure 3. The "top" eigenvalue is positive for a range of $q > 0$ up to a cut-off wave number $q_c = 6.18$ and has a distinct maximum at $q = q_m = 3.88$, which determines a preferred wavelength for the instability. The other, or "bottom" eigenvalue is always stable. Both eigenvalues tend to zero for $q \to 0$. The corresponding eigenfunctions are shown in figure 4. Since eigenfunctions can be rescaled with an arbitrary factor, we can enforce a normalisation condition, which here we chose to be

$$\varphi_1 = 1 \quad \text{at} \quad \xi = 0. \tag{4.15}$$

Interestingly, for $q \to 0$, the eigenfunctions for the two eigenvalues both tend to the translational mode $\varphi_{0\xi}$. This is in contrast to the situation for the static ridge where the eigenfunctions tend to two different eigenfunctions for $q \to 0$, namely the peristaltic mode and the varicose mode. Inspection of the solutions of (4.8) for $\sigma = 0$ and $q = 0$ shows that while the translational mode $\varphi_{0\xi}$ is an eigenfunction for $\sigma = 0$ where $q = 0$, the variation of the base state with respect to rescaling is $\xi\varphi_{0\xi} - \varphi_0$, which is only a generalized eigenfunction, in the sense that plugging it into (4.8a) yields the eigenfunction.

Furthermore, the behavior of $\sigma(q)$ is linear in q for $q \to 0$ for both eigenvalues, i.e. $\sigma(q) \sim \sigma_1|q|$ rather than the $O(q^2)$ leading order behavior that is typically observed for the finger instability in e.g. gravity or Marangoni-driven thin film flows. But see also [45], where, via different arguments, similar behaviour was found for the situation of sliding two-dimensional droplets.

4.3   The long-wave limit

A long-wave expansion that we carry out now reveals that this behaviour is due to the fact that for $q = 0$, the double eigenvalue $\sigma = 0$ has one proper and one generalized eigenfunction, i.e. the long-wave expansion arises as the perturbation of an algebraically double eigenvalue of geometric multiplicity one. We first define L to be the linear differential operator that describes the left hand side of (4.8a), i.e.,

$$L\varphi_1 \equiv \left(\varphi_0^2 \left(\varphi_{1\xi\xi} - q^2\varphi_1 \right)_\xi \right)_\xi - q^2\varphi_0^2 \left(\varphi_{1\xi\xi} - q^2\varphi_1 \right) + \varphi_{1\xi},$$

Furthermore, let L_0 and L_1 be the parts of L that correspond to terms that are respectively independent of and quadratic in q. Also, let L_0^* denote the
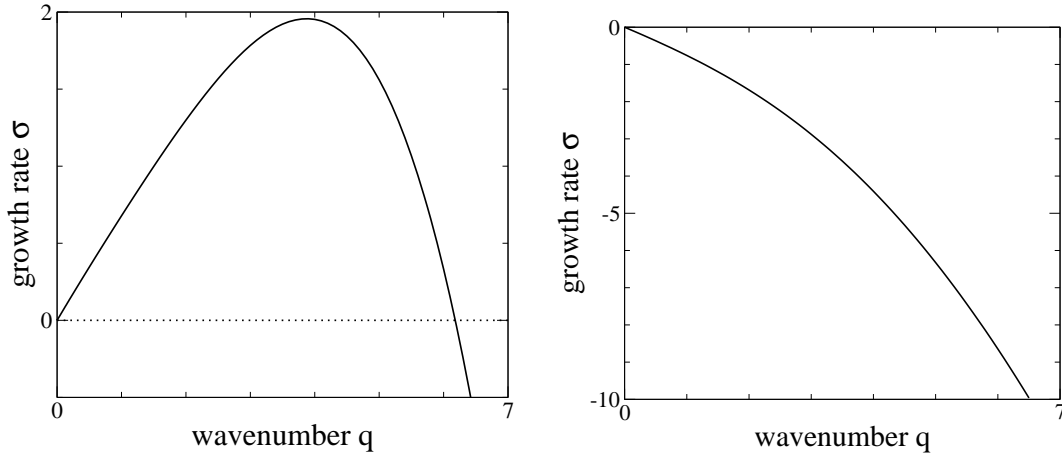
Figure 3: The top eigenvalue ((a), left figure) and the bottom eigenvalue ((b), right figure) in the slip dominated case, i.e. for (4.8).
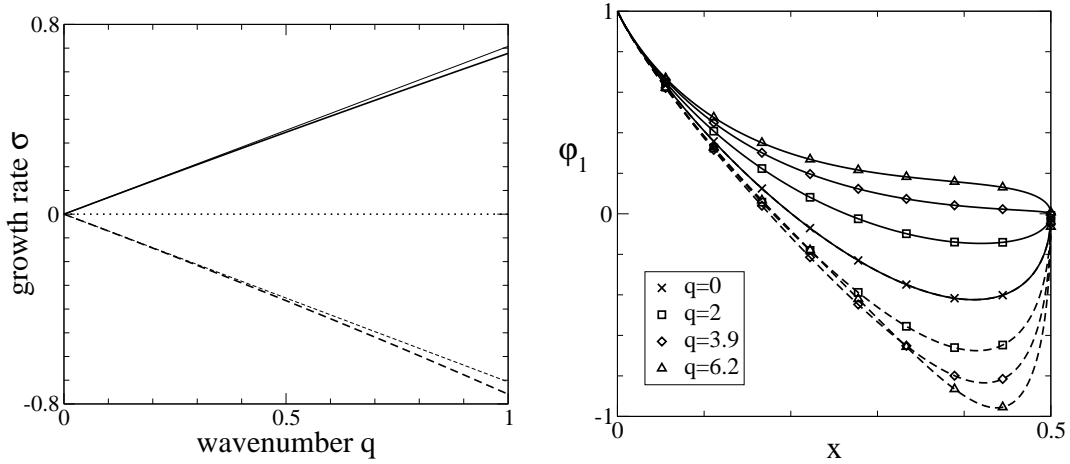

Figure 4: (a) A zoom into the long-wave range (small q) range for the top and bottom eigenvalues. The thicker lines are numerical results for the eigenvalue problem (4.8), the thinner ones come from the long-wave approximation (4.23b). (b) The eigenfunctions for both eigenvalues for a number of different wavenumbers q. Solid lines are used for the eigenfunctions of the top, and dashed lines for those of the bottom, eigenvalue, respectively. The symbols indicate the corresponding value of q. For $q \to 0$, the two lines coincide since both eigenfunctions tend to the translational mode (i.e. to $\varphi_{0,\xi}$).

13

adjoint operator of L_0:

$$L_0\varphi \equiv \left(\varphi_0^2 \varphi_{\xi\xi}\right)_\xi + \varphi_\xi, \tag{4.16a}$$

$$L_1\varphi \equiv -\left(\varphi_0^2 \varphi_\xi\right)_\xi - \varphi_0^2 \varphi_{\xi\xi}, \tag{4.16b}$$

$$L_0^*\psi \equiv \left(\varphi_0^2 \psi_\xi\right)_{\xi\xi} - \psi_\xi. \tag{4.16c}$$

We seek an expansion for the eigenvalues and eigenfunctions σ and φ_1 of (4.8) of interest in terms of q. Motivated by our numerical findings, we make the ansatz (assuming $q \geq 0$):

$$\sigma = \sigma_1 q + \sigma_2 q^2 + O(q^3), \qquad \varphi_1 = \varphi_{0\xi} + \varphi_{11}q + \varphi_{12}q^2 + O(q^3). \tag{4.17}$$

Plugging this ansatz and the expansions of L in (4.16) into $L\varphi_1 = -\sigma\varphi_1$, the leading order terms are zero, while for the $O(q)$ and $O(q^2)$ problems we obtain

$$L_0\varphi_{11} = -\sigma_1\varphi_{0\xi}, \tag{4.18a}$$

$$L_0\varphi_{12} + L_1\varphi_{0\xi} = -\sigma_1\varphi_{11} - \sigma_2\varphi_{0\xi}. \tag{4.18b}$$

Also, we continue to enforce the normalisation condition (4.15) on φ_1, which implies

$$\varphi_{1l} = 0 \quad \text{at} \quad \xi = 0 \quad \text{for} \quad l \geq 1. \tag{4.19}$$

Equation (4.18a) implies that φ_{11} must be the σ_1 multiple of the generalized eigenfunction $\bar{\rho}$, plus an arbitrary multiple of ρ. The arbitrariness is removed by (4.19), and we obtain

$$\varphi_{11} = -\sigma_1 \left(\xi\varphi_{0\xi} - \varphi_0\right). \tag{4.20}$$

We plug this result into (4.18b) and integrate the equation with respect to ξ, which yields,

$$\int_0^{1/2} L_1\varphi_{0\xi}\, d\xi = \sigma_1^2 \int_0^{1/2} \xi\varphi_{0\xi} - \varphi_0\, d\xi \tag{4.21}$$

The integrals on both sides can be evaluated by partial integration, and then we can solve for $\sigma_1^2 = 1/2$, or

$$\sigma_1 = \pm\frac{\sqrt{2}}{2}. \tag{4.22}$$

Together with (4.20) we therefore obtain to $O(q)$ for the branches of eigensolution

$$\sigma = \pm\frac{\sqrt{2}}{2}q, \tag{4.23a}$$

$$\varphi_1 = \varphi_{0\xi} \mp \frac{\sqrt{2}}{2}q\left(\xi\varphi_{0\xi} - \varphi_0\right). \tag{4.23b}$$

The knowledge of the eigenfunctions can be used to determine how the unstable mode perturbs the two boundaries. For a given eigenfunction h_1 for an unstable eigenvalue σ for some q, the left boundary is perturbed by $d_1^- e^{iqy+\sigma t}$,

14

where $d_1^- = -\varphi_1(0)$. This follows from (4.4a), rescaled by (4.7). On the other hand, it follows from equation (4.8c) that $d_1^+ \, e^{iqy+\sigma t}$ is the perturbation of the right boundary, and

$$d_1^+ = \lim_{\xi \to 1/2} \left[\varphi_1/6^{1/2}(1/2 - \xi)^{1/2} \right].$$

Since the eigenfunction φ_1 is given as linear combinations of the functions $\phi_1^\pm$ and $\phi_2^\pm$, the expansions of which we know at the boundaries, the values of $d_1^\pm$ can be expressed in terms of $c_1^\pm$ and $c_2^\pm$. One finds $d_1^- = -c_1^-$ and $d_1^+ = c_1^+/6^{1/2}$, thus

$$d_{\mathrm{rel}} \equiv \frac{d_1^+}{d_1^-} = \frac{c_1^+/6^{1/2}}{-c_1^-}. \tag{4.24}$$

For the translation mode, both boundaries are shifted by the same amount in the same direction, and therefore $d_{\mathrm{rel}} = 1$. The graphs of the eigenfunctions in figure 3 suggest that the contribution of ϕ_1^+ hence c_1^+ decreases as q increases and eventually changes sign. This is indeed the case, as seen in figure 5, where the d_{rel} is shown as a function of q. The function decreases monotonically from one and crosses zero near $q = 3.62$, just below the preferred wavenumber q_m.

For $q > 3.62$, the perturbation of the right boundary is out of phase with the left boundary by half a period, so that rim would be composed by thinner and thicker parts resembling a peristaltic perturbation. However, near $q = 3.62$ the perturbation of the right boundary is nearly zero and even when q approaches the cut-off wavenumber q_c, beyond which the perturbation decays anyway, d_{rel} is less than 0.4 i.e. the perturbation is less than half the size of the left boundary. Hence, all unstable perturbations will appear to be 'asymmetric' in the sense that the side facing the undisturbed film is much less perturbed than the side facing the dewetted area.

The expression (4.24) can be obtained approximately using the long-wave-approximation for the eigenfunction (4.23b), and this leads to

$$d_{\mathrm{rel}} = 1 - \frac{\sqrt{2}}{4} q + O(q^2). \tag{4.25}$$

The corresponding straight line is also shown in figure 5 as a thinner line. It compares well with the numerical result for small and even moderate values of q.

5 Comparison to the full lubrication model

As a next step, we investigate the stability of a growing rim for the full lubrication model in the slip case, given by (2.4), (2.5).

First, we obtain the base state by solving these equations numerically for the case where h does not depend on y, using a slightly smoothed jump as initial data. We use here $\epsilon = 0.04$ and set $\beta = 1$, as well as a slightly modified intermolecular potential

$$\Phi(h) = \Phi_2(h) \equiv \frac{a_1}{8h^8} - \frac{a_2}{2h^2} + \frac{a_3}{2(h+d)^2}, \tag{5.1a}$$

15

with

$$a_1 = 1.014, \quad a_2 = 1.014, \quad a_3 = 7.465, \quad d = 25.34. \tag{5.1b}$$

This three-term potential was motivated by numerical studies in earlier articles [26, 28, 30].

The base profile grows as the rim moves in the direction of the unperturbed film, see figure 6(a). From the scalings in (3.2), we see that the growth of the height and width of the rim is inversely proportional to the dewetting rate $c = \dot{s}$. Thus, the dewetting rate decreases as the rim moves further into the unperturbed film. In fact, a specific law for the evolution of the contact line region, $s(t) \sim t^{2/3}$, can be found from the rescalings (3.2) and a mass balance argument. Derivations and discussions of this law can be found in the literature [4, 13, 30, 34, 36].

The rescalings (3.2) of the traveling wave solution in section 3 lead to a universal profile φ_0 without any free parameters. Hence, if we rescale the profiles in figure 6(a) that were obtained for the full lubrication model according to (3.2), we expect the result to closely approximate φ_0. Instead of obtaining c from the evolution of the contact line, we rescale h by $\max_x(h(x,t))/\max_\xi(\varphi(\xi))$; the corresponding lateral length scale is found by comparison with (3.2). Hence, we rescale according to

$$h = \frac{\max_x(h(x,t))}{\max_\xi(\varphi_0(\xi))}\hat{\varphi} \qquad x = \frac{\max_x(h(x,t))}{\lambda \max_\xi(\varphi_0(\xi))}\xi. \tag{5.2}$$

The result is shown in figure 6(b). We clearly see that the rescaled solutions of the full lubricaiton model converge, for later times, onto the normalized traveling solution φ for the sharp interface model, i.e. of (3.3). This is to be expected, since for later times, the rim is larger and hence the residual film and the unperturbed film thickness are smaller relative to the rim height, and this means the effective ϵ and β are smaller.

As next step we describe the occurrence of fingers in the ridge for the full lubrication model in terms of the evolution of a small perturbation of the base state which we now denote by $h_{\mathrm{b}}(x,t)$. Specifically, we introduce the perturbation

$$h(x,y,t) = h_{\mathrm{b}}(x,t) + \delta h_{\mathrm{p}}(x,t)\exp(iky)$$

into the lubrication model, with $\delta \ll 1$ and retain only linear terms in δ. We obtain for the linearized equation

$$\frac{\partial h_{\mathrm{p}}}{\partial t} + \mathcal{L}h_{\mathrm{p}} - k^2 \left[\left(h_{\mathrm{b}}^2 h_{1x}\right)_x + h_{\mathrm{b}}^2 \left(h_{1xx} - \varepsilon^{-2}\Phi''\left(h_{\mathrm{b}}/\varepsilon\right)\right) \right]$$
$$+k^4 h_{\mathrm{b}}^2 h_{\mathrm{p}} = 0, \quad (5.3)$$

where

$$\mathcal{L}h_{\mathrm{p}} \equiv \frac{\partial}{\partial x}\left[2h_{\mathrm{b}}^2\right)\left(h_{\mathrm{b}xxx} - \varepsilon^{-2}\Phi''\left(h_{\mathrm{b}}/\varepsilon\right)\right)h_{\mathrm{b}x}\right) h_{\mathrm{p}} - h_{\mathrm{b}}^2\,\varepsilon^{-2}\Phi''\left(h_{\mathrm{b}}/\varepsilon\right)\,h_{\mathrm{b}x}h_{\mathrm{p}}$$
$$+h_{\mathrm{b}}^2\left(h_{1xxx} - \varepsilon^{-2}\Phi''\left(h_{\mathrm{b}}/\varepsilon\right)h_{1x}\right)\right] \tag{5.4}$$

Note that since we have a time dependent base state, the coefficients of the linearized PDE are non-constant in time, hence solutions for the linearized
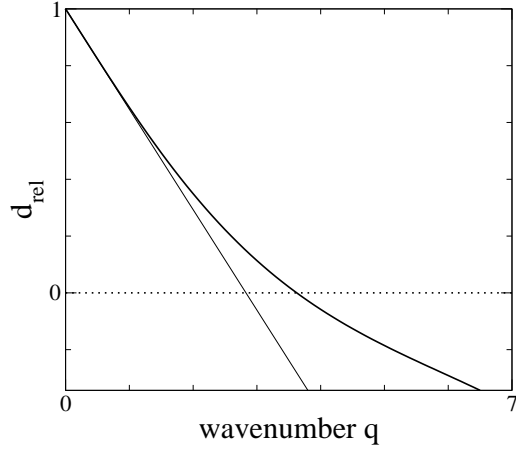
16

Figure 5: The perturbation of the right boundary relative to the perturbation of the left boundary, obtained from the eigenfunction for the top eigenvalue via (4.24), for a range of different wave numbers q. The thicker, curved line is obtained by evaluating (4.24) using the numerically computed eigenfunctions, while the thinner line uses the long-wave approximation, i.e. the formula given in (4.25). Further explanations are given in the text.
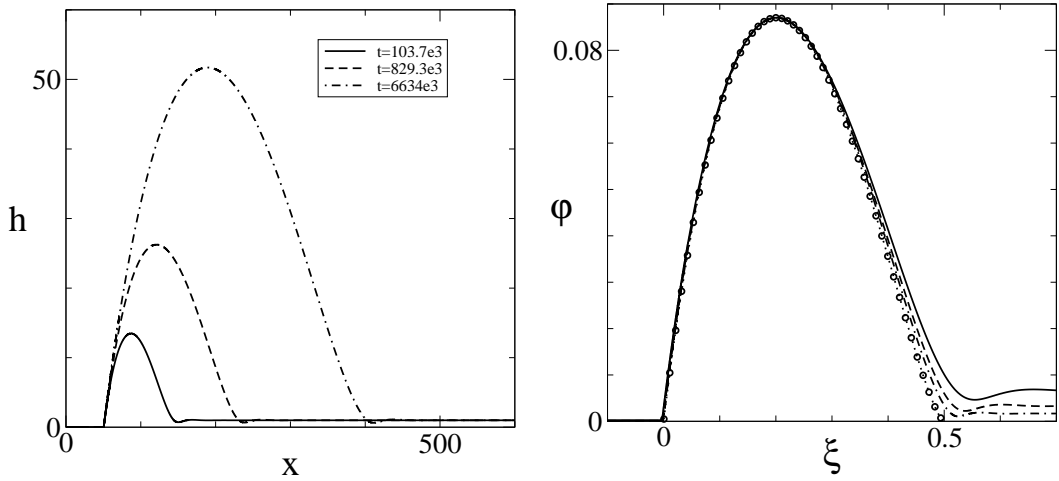

Figure 6: (a) Evolution of the dewetting rim profile obtained by solving (2.4), (2.5) (for only one spatial variable x), with $\epsilon = 0.04$ and $\beta = 1$. The potential is given by (5.1). The figure shows the rim at three different times t. (b) The same rim profiles rescaled as explained in the text, see equation (5.2), using the same line styles as on the left. The fourth profile, shown by open circles, corresponds to the solutions φ for the sharp interface model, see also figure 2.

problem cannot be obtained via a classical eigenvalue approach. Instead, we numerically solve an initial value problem for (5.3), (5.4) for a fixed set of wavenumbers, in tandem with the equation for the base state, and observe how the perturbations evolve in time. The computational effort scales roughly linearly with the number of wave-numbers we monitor.

The evolution is computed for a time interval $[t_0, t_1]$ where t_0 and t_1 are the times where the unperturbed front, more specifically, the left contact line regions, estimated for the purpose of this subsection by the position of the turning point, has reached a certain position, namely

$$s(t_0) = 0.883 \qquad \text{and} \qquad s(t_1) = 1.48 \cdot 10^4;$$

the corresponding times are

$$t_0 = 5.18 \qquad \text{and} \qquad t_1 = 9.85 \cdot 10^6.$$

An initial perturbation $h(t)$ is introduced at time t_0 using the following expression:

$$h_{\mathrm{p}}(x, t_0) = \frac{\partial h_{\mathrm{b}}}{\partial x}(x, t_0), \qquad (5.5)$$

which corresponds to a 'zig-zag' perturbation, i.e. we perturb both sides of the ridge in the same direction [5]. For zero wave-number, (5.5) simply represents an infinitesimal initial shift of the whole profile. Below, we also make some remarks on other choices of the initial data for h_{p}.

To describe the growth of bumps and eventually fingers in the ridges, we use the amplification $A(t)$ of the perturbation with respect to the initial state,

$$A(t) \equiv \frac{\max_x |h_{\mathrm{p}}(x, t)|}{\max_x |h_{\mathrm{p}}(x, t_0)|} \qquad \text{for} \quad t_0 \le t \le t_1.$$

We compare amplifications achieved at the same position of the dewetting fronts, rather than at the same value of t. Figure 7 displays $A(t)$ vs. the front position $s(t)$ for several wavelengths $l = 2\pi/k$. For each of the depicted wavelengths, the perturbation grows as the dewetting proceeds, then it reaches a maximum, after which it decays. Longer wavelengths achieve the maximal amplification factor

$$A_{\max} \equiv \max_{t \ge t_0} A(t)$$

at later stages of the dewetting, when the front has advanced further into the film and the ridge of the base state has grown in size, suggesting that the most amplified wavelength correlates with the width of the ridge [25]. This coincides interestingly with results on the fingering in gravity and Marangoni-driven flows, where the most amplified wavelength in the modal analysis is proportional to the length scale imposed by the bump width [46], and with predictions for the breaking up of static ridges [5] into droplets.

Figure 7(b) shows profiles of the perturbation h_{b} for a fixed choice of $k = 0.0237$ at different stages of amplification. The initial perturbation (given by (5.5)), which has one pronounced maximum and a minimum, slowly evolves into a new profile where the minimum is replaced by a relatively flat part with a weak tendency to create a second 'bump' in the profile of the perturbation
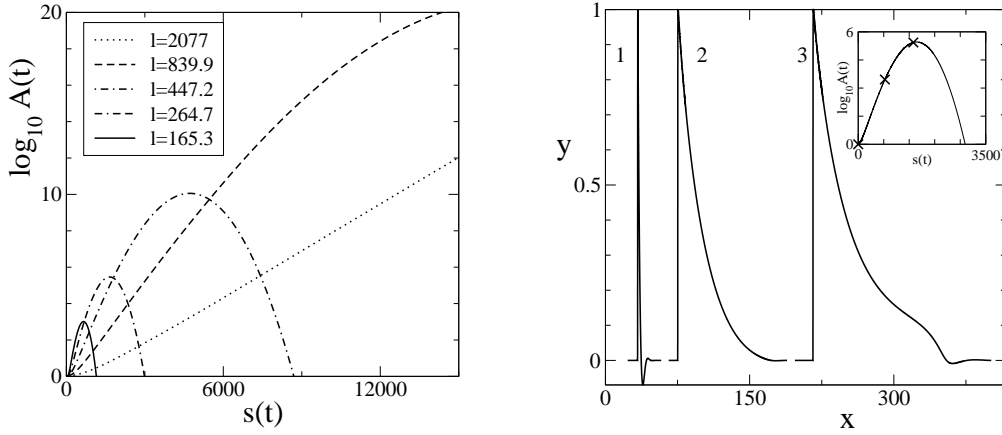
18

Figure 7: (a) Amplification $A(t)$ of the perturbation versus front position $s(t)$. Line styles correspond to different wavelengths $l = 2\pi/k$ as indicated in the legend. (b) The perturbation profile for wavelength $l = 264.7$ at different stages of its evolution, shifted along the x-axis for better distinction, and with the maximum normalized to one. The labels 1, 2, 3 correspond to the crosses in the inset, which indicate the position $s(t)$ of the base state and the amplification $A(t)$ achieved by $h_{\mathrm{p}}(x,t)$.
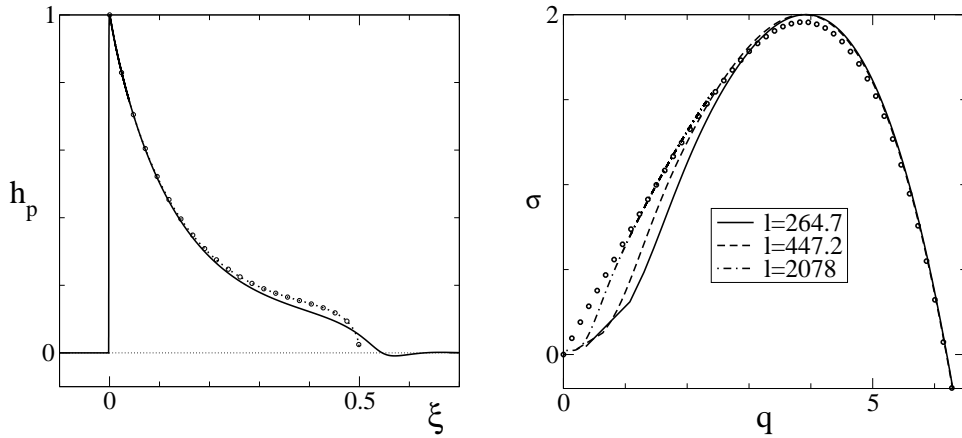

Figure 8: (a) Comparison of the rescaled perturbation $h_{\mathrm{p}}(x,t)$ labelled '2' (solid line) with the eigenfunction of the sharp interface model for the corresponding wavenumber q (circles). (b) Comparison of the rescaled growth rates $\hat{\sigma}$ and wavenumbers q obtained from the solutions h_{p} for several choices of fixed $l = 2\pi/k$, with the dispersion relation for the sharp interface model (circles). Further explanations for (a) and (b) are given in the text.

19

after the maximum amplification has been achieved. This clearly resembles observations made earlier for the eigenfunctions of the linearized sharp interface model.

In fact, we can compare the shape of the perturbation with the eigenfunction in a similar way as before for the base state. We rescale x into ξ as in the second part of (5.2), leaving h_{p} normalized so that the maximum is one. Also, we need to determine the wavenumber for which to take the eigenfunction of the linearized sharp interface model. This is found by scaling k with the inverse of the scale for x,

$$k = \frac{\lambda \, \max_\xi(\varphi_0(\xi))}{\max_x(h(x,t))} q. \tag{5.6}$$

For the h_{p}-profile labelled '2' in figure 7(b), we obtain $q = 6.02$ which is very close to the cut-off wavenumber for the sharp interface model. Note that since $\max_x(h(x,t))$ increases with time, the "effective" wavenumber q decreases with time, and in fact, at the time $t_{\max}$ when $A(t)$ reaches its maximum value $A_{\max}$, which is slightl after the time of profile '2', the value for q turns out to approximate the cut-off wavenumber very closely.

In figure 8, we now compare the rescaled h_{p}-profile with the eigenfunction of (4.8) for $q = 6.02$. We see good agreement for $\xi < 0.2$ but some deterioration as ξ approaches $1/2$. In general, however, we can expect the agreement to improve if we start with a larger $l = 2\pi/k$, since then the base profiles are larger when a certain value of q is reached, hence the thickness of the residual and the unperturbed film thickness are smaller compared to the size of the rim.

Furthermore, note that the evolution of the base state $h_{\mathrm{b}}(x,t)$ is algebraic and thus slow compared to the rapid exponential growth of an unstable mode of (4.3). This suggests that the evolution of h_{p} is given at every instance by solving (4.3) for the most unstable mode. This means in particular that we treat $c = \dot{s}(t)$ as a constant for the purpose of solving (4.3), but retain its slow algebraic growth in the solution itself, in the sense of a "quasistatic" approximation. This yields

$$h_1(x,t) = \frac{\lambda^3}{c} \varphi_1(\xi;q) \exp\left[\frac{c^2}{\lambda^2}\sigma t\right], \quad \xi = \frac{c}{\lambda^2}(x - s), \quad q = \frac{\lambda^2}{c}k, \tag{5.7}$$

where φ_1 and σ represent the eigensolution of (4.8) with the largest real part of σ. Recall that since the wave number k of the perturbation of the full lubrication model is kept fixed, q now changes due to the quasi-static evolution of $c = c(t) = \dot{s}$.

Rather than comparing (5.7) directly with h_{p} we solve (5.7) to express σ in terms of a normalized maximum of h_1,

$$\sigma = \frac{\lambda^2}{c^2} \frac{d}{dt} \ln\left[\frac{\max_x h_1(x,t)}{\max_x h_1(x,t_0)}\right]. \tag{5.8}$$

and then replace h_1 by h_{p}, i.e. we monitor

$$\hat{\sigma} = \hat{\sigma}(t) = \frac{\lambda^2}{c^2} \frac{d}{dt} \ln A(t;k). \tag{5.9}$$

20

The expression $\hat{\sigma}$ can be evaluated in time using the numerical solutions for h_{p} for an arbitrary fixed choice of k. We note that it is convenient to avoid determining $c(t) = \dot{s}(t)$, so we proceed as for the rescaling of the base state and use (5.2), (5.6). The corresponding time scale can be found by comparison with (3.2), so that we actually compute $\hat{\sigma}$ via

$$\hat{\sigma} = \left[\frac{\max_x(h(x,t))}{\lambda^2 \max_\xi(\varphi_0(\xi))} \right]^2 \frac{d}{dt} \ln A(t; k). \tag{5.10}$$

to generate the lines in figure 8(b).

If h_{p} is indeed well approximated by h_1, then the dispersion relation $(q, \sigma(q))$ obtained from the eigenproblem (4.8) must be well approximated by the curve $(q(t), \hat{\sigma}(t))$. In fact, we can argue similarly as before that $(q(t), \hat{\sigma})$ is expected to asymptotically approach $(q, \sigma(q))$ as we consider larger t for the same fixed k, which means larger $q(t)$ or repeat the procedure with a larger choice for k. Indeed, this is what we see in figure 8(b).

6   Conclusion

In this paper we derived the sharp-interface model for a dewetting rim from the corresponding lubrication model taking account of slippage. For the resultig reduced model we were able to derive analytical expressions for the dispersion relations that show that the dependence of the growth rate on the wavenumber is linear. This is in contrast to the quadratic denpendence typically found for finger-type instabilities in thin film problems. It is therefore interesting to investigate via the methods of this study the linear stability of the sharp-interface model corresponding to the typically used no-slip case. This will be the topic of a companion paper to follow.

Acknowledgements

References

[1] A. L. Bertozzi and M. P. Brenner. Linear stability and transient growth in driven contact lines. *Phys. Fluids*, 9:530–539, March 1997.

[2] A. L. Bertozzi, A. Münch, X. Fanton, and A. M. Cazabat. Contact line stability and 'undercompressive shocks' in driven thin film flow. *Phys. Rev. Lett.*, 81:5169–5172, December 1998.

[3] F. Brochard-Wyart, P.-G. de Gennes, H. Hervert, and C. Redon. Wetting and slippage of polymer melts on semi-ideal surfaces. *Langmuir*, 10:1566–1572, 1994.

[4] F. Brochard-Wyart, G. Debregeas, R. Fondecave, and P. Martin. Dewetting of supported viscoelastic polymer films: Birth of rims. *Macrom.*, 30:1211, 1997.

[5] F. Brochard-Wyart and C. Redon. Dynamics of liquid rim instabilities. *Langmuir*, 8:2324–2329, 1992.

[6] J. B. Brzoska, F. Brochard-Wyart, and F. Rondelez. Exponential growth of fingering intabilities of spreading films under horizontal thermal gradients. *Europhysics Letters*, 19:97–102, 1992.

[7] R. Buckingham, M. Shearer, and A. Bertozzi. Thin film traveling waves and the Navier-slip condition. *SIAM J. Appl. Math.*, 63:722–744, 2003.

[8] A. M. Cazabat, F. Heslot, S. M. Troian, and P. Carles. Finger instability of this spreading films driven by temperature gradients. *Nature*, 346(6287):824–826, 1990.

[9] J. W. Evans. Nerve axon equations: I. *Ind. Univ. Math. J.*, 21:877–885, 1972.

[10] J. W. Evans. Nerve axon equations: II. *Ind. Univ. Math. J.*, 22:75–90, 1972.

[11] J. W. Evans. Nerve axon equations: III. *Ind. Univ. Math. J.*, 22:577–593, 1972.

[12] J. W. Evans. Nerve axon equations: IV. *Ind. Univ. Math. J.*, 24:1169–1190, 1975.

[13] J. C. Flitton and J. R. King. Surface-tension-driven dewetting of Newtonian and power-law fluids. *J. Engr. Math.*, 50:241–266, 2005.

[14] N. Garnier, R. O. Grigoriev, and M. F. Schatz. Optical manipulation of microscale fluid flow. *Phys. Rev. Lett.*, 91:054501, 2003.

[15] K. B. Glasner. Spreading of droplets under the influence of intermolecular forces. *Phys. Fluids*, 17:1837–1842, 2003.

[16] K. B. Glasner. A boundary integral formulation of quasi-steady fluid wetting. *J. Comp. Phys.*, 207:529–541, 2005.

[17] K. B. Glasner. Variational models for moving contact lines and the quasi-static approximation. *Euro. J. Appl. Math*, 16:1–28, 2005.

[18] A. C. Hindmarsh. ODEPACK, a systematized collection of ODE solvers. In R. S. Stepleman et al., editors, *Scientific Computing*, volume 1 of *IMACS Transactions on Scientific Computation*, pages 55–64. North-Holland, Amsterdam, 1983.

[19] H. Huppert. Flow and instability of a viscous current down a slope. *Nature*, 300:427–429, 1982.

[20] K. Jacobs, R. Seemann, G. Schatz, and S. Herminghaus. Growth of holes in liquid films with partial slippage. *Langmuir*, 14:4961–4963, 1998.

[21] D. E. Kataoka and S. M. Troian. A theoretical study of instabilities at the advancing front of thermally driven coating films. *J. Coll. Int. Sci.*, 192:350–362, 1997.

[22] J. King, A. Münch, and B. A. Wagner. Linear stability of a ridge. *Non-linearity*, 19:2813–2831, 2006.

[23] R. Konnur, K. Kargupta, and A. Sharma. Instability and morphology of thin liquid films on chemically heterogeneous substrates. *Phys. Rev. Lett.*, 84:931–934, 2000.

[24] P. G. López, S. G. Bankoff, and M. J. Miksis. Non-isothermal spreading of a thin liquid film on an inclined plane. *J. Fluid Mech.*, 11:1–39, 1996.

[25] J.-L. Masson, O. Olufokunbi, and P. F. Green. Flow instabilities in entangled polymer films. *Macrom.*, 35:6992–6996, 2002.

[26] A. Münch. Fingering instability in dewetting films induced by slippage. MATHEON preprint number 123, 2004.

[27] A. Münch. Dewetting rates of thin liquid films. *J. Phys. C*, 17:309–318, 2005.

[28] A. Münch and B. Wagner. Contact-line instability of dewetting thin films. *Physica D*, 209:178–190, 2005.

[29] A. Münch and B. A. Wagner. Numerical and asymptotic results on the linear stability of a thin film spreading down a slope of small inclination. *Euro. J. Appl. Math.*, 10:297–318, 1999.

[30] A. Münch, B. A. Wagner, and T. P. Witelski. Lubrication models with small to large slip lengths. *J. Eng. Math.*, 53:359–383, 2006.

[31] C. Neto and K. Jacobs. Dynamics of hole growth in dewetting polystyrene films. *Physica A*, 339:66–71, 2004.

[32] A. Oron, S. H. Davis, and S. G. Bankoff. Long-scale evolution of thin liquid films. *Rev. Mod. Phys.*, 69:931–980, 1997.

[33] C. Redon, F. Brochard-Wyart, and F. Rondelez. Dynamics of dewetting. *Phys. Rev. Lett.*, 66:715–718, 1991.

[34] C. Redon, J. B. Brzoska, and F. Brochard-Wyart. Dewetting and slippage of microscopic polymer films. *Macrom.*, 27:468–471, 1994.

[35] G. Reiter. Dewetting of thin polymer films. *Phys. Rev. Lett.*, 68:75–78, 1992.

[36] G. Reiter and R. Khanna. Kinetics of autophobic dewetting of polymer films. *Langmuir*, 16:6351–6357, 2000.

[37] G. Reiter and A. Sharma. Auto-optimization of dewetting rates by rim instabilities in slipping polymer films. *Phys. Rev. Lett.*, 80:166103, 2001.

[38] G. Reiter, A. Sharma, A. Casoli, M.-O. David, R. Khanna, and P. Auroy. Thin film instability induced by long-range forces. *Langmuir*, 15:2551–2558, 1999.

[39] R. Seemann, S. Herminghaus, and K. Jacobs. Dewetting patterns and molecular forces: A reconciliation. *Phys. Rev. Lett.*, 86:5534–5537, 2001.

[40] R. Seemann, S. Herminghaus, and K. Jacobs. Gaining control of pattern formation of dewetting films. *J Phys. C*, 13:4925–4938, 2001.

[41] A. Sharma and R. Khanna. Pattern formation in unstabile thin liquid films. *Phys. Rev. Lett.*, 81(16):3463–3466, 1998.

[42] A. Sharma and R. Khanna. Pattern formation in unstable thin liquid films under influence of antagonistic short- and long-range forces. *Journal of Chemical Physics*, 110(10):4929–4936, 1999.

[43] A. Sharma and G. Reiter. Instability of thin polymer films on coated substrates: Rupture, dewetting and drop formation. *J. Coll. Int. Sci.*, 178:383–389, 1996.

[44] N. Silvi and E. D. V. On the rewetting of an inclined solid surface by a liquid. *Phys. Fluids*, 28:5–7, 1985.

[45] U. Thiele and E. Knobloch. Front and back instability of a liquid film on a slightly inclined plane. *Phys. Fluids*, 15:892–907, 2003.

[46] S. M. Troian, E. Herbolzheimer, S. A. Safran, and J. F. Joanny. Fingering instabilities of driven spreading films. *Europhys. Lett.*, 10:25–30, 1989.

[47] E. O. Tuck and L. W. Schwartz. A numerical and asymptotic study of some third-order ordinary differential equations relevant to draining and coating flows. *SIAM Review*, 32:453–469, 1990.

[48] R. Xie, A. Karim, J. F. Douglas, C. C. Han, and R. A. Weiss. Spinodal dewetting of thin polymer films. *Phys. Rev. Lett.*, 81:1251–1254, 1998.